Arsenic Monolayers Formed by Zero-Dimensional Tetrahedral Clusters and One-Dimensional Armchair Nanochains

Guowei Liu,[#] Shao-Gang Xu,[#] Yaping Ma,* Xiji Shao, Wenqi Xiong, Xuefeng Wu, Shuxuan Zhang, Chenwei Liao, Congrun Chen, Xixian Wang, Shengjun Yuan, Weifeng Zhang, Jiong Lu, Hu Xu,* Kedong Wang,* and Xudong Xiao*

Cite This: *ACS Nano* 2022, 16, 17087−17096 | Read Online

ACCESS | Metrics & More | Article Recommendations | SI Supporting Information

ABSTRACT: One-dimensional (1D) arsenene nanostructures are predicted to host a variety of interesting physical properties including antiferromagnetic, semiconductor–semimetal transition and quantum spin Hall effect, which thus holds great promise for next-generation electronic and spintronic devices. Herein, we devised a surface template strategy in a combination with surface-catalyzed decomposition of molecular As_4 cluster toward the synthesis of the superlattice of ultranarrow armchair arsenic nanochains in a large domain on Au(111). In the low annealing temperature window, zero-dimensional As_4 nanoclusters are assembled into continuous films through intermolecular van der Waals and molecule–substrate interactions. At the elevated temperature, the subsequent surface-assisted

decomposition of molecular As_4 nanoclusters leads to the formation of a periodic array of 1D armchair arsenic nanochains that form a (2×3) superstructure on the Au(111) surface. These ultranarrow armchair arsenic nanochains are predicted to have a small bandgap of ∼0.50 eV, in contrast to metallic zigzag chains. In addition, the Au-supported arsenic nanochains can be flipped to form a bilayer structure through tip indentation and manipulation, suggesting the possible transfer of these nanochains from the substrate. The successful realization of arsenic nanostructures is expected to advance low-dimensional physics and infrared optoelectronic nanodevices.

KEYWORDS: one-dimensional nanostructures, arsenic molecular film, arsenic nanochain, scanning tunneling microscopy, tip indentation and manipulation
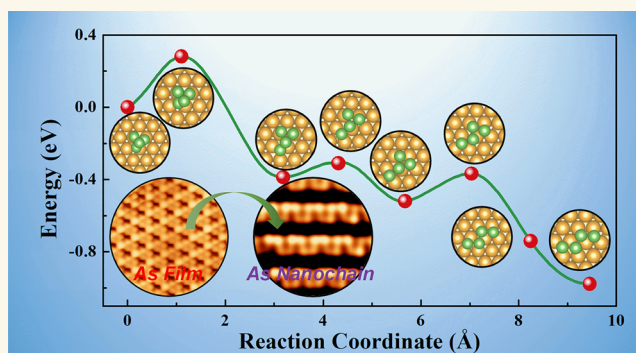
Two-dimensional (2D) materials have attracted great attention due to their distinct physical and chemical properties for various potential applications.[1−5] Ever since the discovery of graphene,[6,7] various 2D materials,[8−11] including transition metal dichalcogenides (TMDs),[12] silicene,[13] borophene,[14] germanene,[15] and phosphorene,[16] have been synthesized. Moreover, many attempts have been made to create quasi-one-dimensional (quasi-1D) materials aimed at fine-tuning the physical properties.[17−21] For instance, despite the outstanding electronic properties of graphene, its gapless band structure severely limits its potential applications in electronic devices. To circumvent such a constraint, graphene nanoribbons (NRs) exhibiting semiconductor properties by quantum confinement were often constructed.[17,19]

As representative nanostructures in group V elements, phosphorene and phosphorene NRs have been widely studied.[2,21,22] In particular, phosphorene NRs or nanochains can be obtained by top-down and bottom-up methods, including ionic scissoring,[22] electrochemical exfoliation,[23] and molecular beam epitaxy (MBE).[21] Phosphorene nanoribbons have been theoretically predicted to possess peculiar physical properties, such as Stark and Seebeck effects,[24,25] room temperature magnetism,[26] and topological phase transition.[27] Similarly, antimonene NRs have been successfully grown by MBE on sapphire(0001) and Ag(111) surfaces[28,29] and by
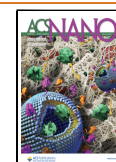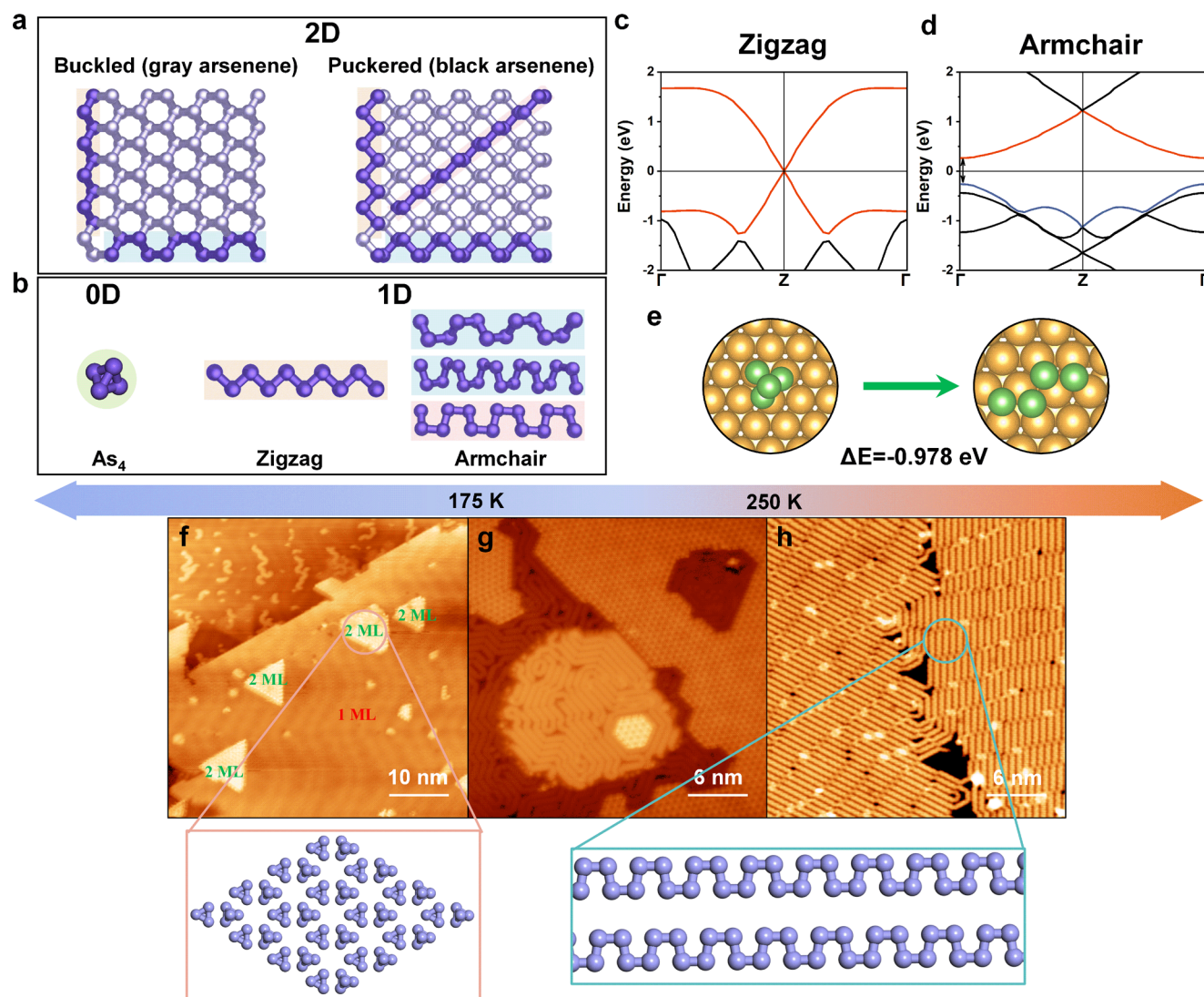
Figure 1. Schematic illustration of various low-dimensional arsenic nanostructures and the synthetic strategy of 1D arsenic nanostructures. (a) 2D arsenene. (b) 0D and 1D arsenic nanostructures. (c, d) Calculated band structures of flat (c) metallic zigzag and (d) semiconducting armchair nanochains. (e) Decomposition from an As_4 molecule to an arsenic segment for the synthesis of 1D arsenic nanochains. (f−h) Schematic diagram of substrate temperature dependent arsenic nanostructures. (f) STM image ($V_{bias} = -1$ V, $I_t = 10$ pA) of arsenic film composed of 0D As_4 molecules deposited below 175 K. The triangle islands are the second layer of As_4 molecular film which has the same structure as the first layer. (g) STM image ($V_{bias} = 50$ mV, $I_t = 500$ pA) of arsenic deposited on the Au(111) substrate from 175 to 250 K. Arsenic nanochain structures are formed through the decomposition of As_4 molecules. (h) STM image ($V_{bias} = 10$ mV, $I_t = 1$ nA) of arsenic nanochains grown in the temperature range of 250−600 K.

plasma-assisted process on InSb.[30] It is interesting to find that the edge structures of antimonene NRs can dramatically affect their physical properties,[31,32] which can be modulated by electric field[33−35] and gas molecular adsorption,[36] demonstrating great potential applications in nanoelectronics and toxic gas sensors. Arsenic belongs to the same group of chemical elements and serves as the main raw material for many arsenide semiconductors. The sp^3 hybridization of arsenic produces plenty of possible structures at the nanoscale, such as nanosheet, nanoribbon, nanotube, nanoring, arsenene, and so on.[37−40] For 2D arsenic nanostructures (Figure 1a), theoretical studies have predicted that 2D arsenene has various properties, notably indirect-to-direct bandgap transition,[41,42] semimetal-to-semiconductor transition,[42] quantum spin Hall effect,[43−45] and superconductivity.[46] Liquid phase exfoliation and mechanical exfoliation of arsenic were predominantly used to prepare 2D arsenic.[47,48] Recently, Shah et al. have reported

the growth of monolayer arsenene on Ag(111) surface by sublimation of arsenic from InAs onto a heated substrate at 523−623 K.[39] Using a sample of few-layer black arsenic, the particle-hole asymmetric Rashba valley and exotic quantum Hall states were recently observed due to the synergetic effects between spin−orbit interaction and the Stark effect.[48] For zero-dimensional (0D) arsenic nanostructures, 0D As_4 molecule (tetrahedral molecular structure composed of four arsenic atoms in Figure 1b) called yellow arsenic, which is very unstable and prefers to transform into gray arsenic under ambient condition, can only be synthesized in solution.[49] For 1D arsenic nanostructures, arsenene can be sliced into 1D or quasi-1D arsenic nanochains or nanoribbons (Figure 1b) with zigzag or armchair edge. It has been theoretically predicted that the armchair nanoribbons possess tunable electronic properties that can be modulated by the nanoribbon width, strain, and electric field (Figure 1d) while the semimetallic zigzag
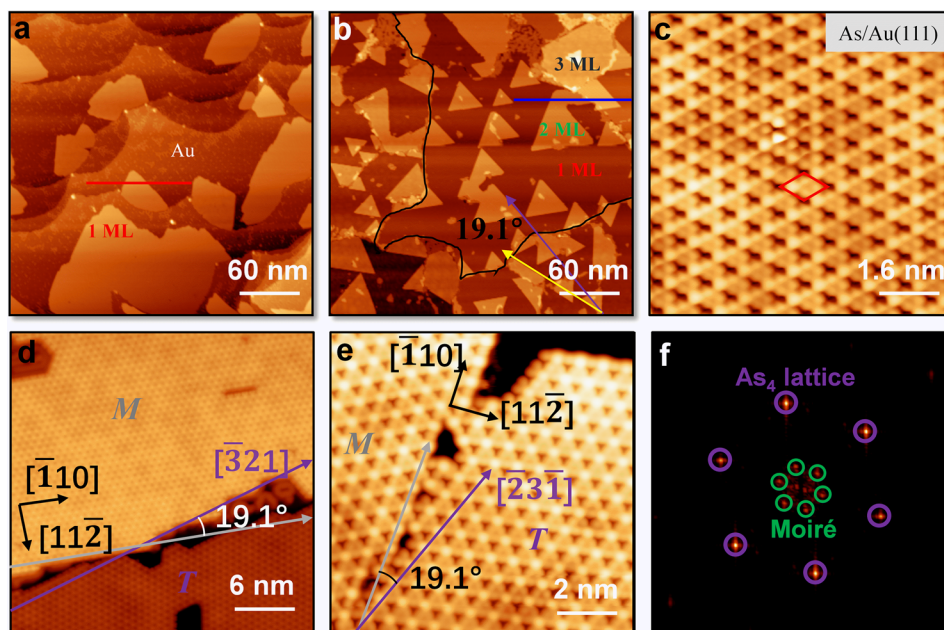
Figure 2. Structures of arsenic molecular films (*M*-phase and *T*-phase) on Au(111) grown below 175 K. (a, b) Large-scale STM images (V_{bias} = 2.0 V, I_t = 10 pA) of about (a) 0.5 ML and (b) 1.5 ML arsenic films on Au(111). (c) High-resolution STM image (V_{bias} = 50 mV, I_t = 300 pA) of arsenic film on Au(111). (d) Large-scale (V_{bias} = 0.1 V, I_t = 500 pA) and (e) the high-resolution STM images (V_{bias} = −0.2 V, I_t = 500 pA) reveal the boundary between two arsenic phases. (f) FFT image of *M*-phase arsenic films. The hexagonal patterns marked by purple and green circles correspond to the periodicities of As$_4$ molecular film and Moiré pattern, respectively.

nanoribbons (Figure 1c) exhibit antiferromagnetic properties by considering the magnetic interaction between the edge states.[50−52] Moreover, a transverse electric field can possibly induce band inversion to lead to a nontrivial topological phase which should manifest in the quantum spin Hall effect.[50] Experimentally, multilayer gray and black arsenene nanoribbons have been prepared for the potential applications in light-emitting and thermoelectric devices, respectively.[53,54] Nevertheless, the growth of monolayer or few-layer 1D arsenic nanochains or quasi-1D arsenic nanoribbons has rarely been reported for further studies.[2,53,55,56]

Here, we realize the synthesis of large-size ordered armchair-like arsenic nanochains on the Au(111) surface by a surface template strategy. It has been found that high-quality monolayer As$_4$ molecular films and nanochains could be grown on Au(111) surface at different substrate temperatures by thermally evaporating a bulk gray As source. At low temperatures (≤175 K), the deposited arsenic on Au(111) surface was found in the form of As$_4$ molecules but decomposed into atomic segments at high temperatures (250−600 K). Using scanning tunneling microscopy/spectroscopy (STM/STS) and density functional theory (DFT) calculations, the structures and electronic properties of the arsenic films and nanochains were carefully investigated. The arsenic films are formed by two alternatively arranged molecular As$_4$ nanoclusters in one unit cell, and the arsenic nanochains are formed by atomic arsenic with high stability due to the decomposition of As$_4$ molecules by Au(111). The high-quality arsenic nanochains can organize over a vast surface of tens of thousands of square nanometers and demonstrate an armchair structure to form a (2 × 3) superstructure of Au(111) surface. These freestanding ultra-narrow armchair arsenic nanochains are calculated to have a small bandgap of ~0.50 eV, suitable for the applications of electronic and infrared optoelectronic devices. Furthermore,

the flip of arsenic nanochains by tip indentation and manipulation demonstrates the feasible exfoliation of arsenic nanochains for future nanodevice fabrications.

RESULTS AND DISCUSSION

As$_4$ molecule-like nanocluster is the main species through the evaporation of bulk gray arsenic.[49] The decomposition of such As$_4$ nanocluster into arsenic segment can lead to the formation of 1D arsenic nanostructures. It has been calculated that the total energy of an arsenic nanochain on Au(111) surface is much lower than that of an As$_4$ molecule on Au(111) surface (Figure 1e and Figure S1b), suggesting the synthesis of 1D arsenic nanostructures via surface template strategy. Apart from this, substrate-induced charge transfer often tends to stabilize the surface for supporting low-dimensional nanostructures, as reflected in previous studies.[57,58] Therefore, we first used the thermal evaporation for the deposition of arsenic source on Au(111) surface, which can be used for the subsequent 1D nanochain formation. It is noted that the morphologies of the grown arsenic nanostructures strongly depend on the temperature of gold substrate (Figure 1f−h). Specifically, the substrate temperature can modulate the surface-assisted effect of Au(111) on the decomposition of As$_4$ molecules to produce different arsenic precursors, leading to the formation of various arsenic nanostructures. With elevation of the substrate temperature, the arsenic nanostructures undergo an evolution from molecular film of As$_4$ assembled by van der Waals forces to 1D nanochains (the atomic structure of these two different structures will be discussed in detail later). At low substrate temperatures (≤175 K), only a well-ordered arsenic molecular film can be obtained (Figure 1f); when the substrate temperature reaches the range from 175 to 250 K, arsenic molecular film and nanochains can coexist on the substrate (Figure 1g). After the substrate temperature increases to above 250 K, large areas of arsenic

nanochains are formed without any more arsenic molecular films (Figure 1h). When the substrate temperature goes higher than 600 K, the adsorption of arsenic on Au(111) surface is strongly inhibited with only some residual arsenic islands remaining on the surface (Figure S2). In the following, we will focus on the presentation of arsenic films and arsenic nanochains.

Figure 2a,b shows the STM images of ~0.5 monolayer (ML) and ~1.5 ML of arsenic deposited on the Au(111) at 175 K. The ordered arsenic islands prefer to follow a step-flow growth mode until it covers the whole terraces. This adlayer growth mode differs from the etching growth mode of P on Au(111),[59,60] demonstrating that the arsenic film is unlikely to be an alloy. Furthermore, the arsenic film shows two different domain orientations with an angle difference of 19.1°, as shown in Figure 2b. The second and third arsenic layers follow the direction of the underneath first layer. The above angle difference of 19.1° between domains is consistent with the angle between $[\bar{1}10]$ and $[2\bar{3}\bar{1}]$ directions on Au(111) surface (Figure 2d,e and Figure S3). The arsenic film with one edge along $[\bar{1}10]$ shows clear Moiré patterns (top part of Figure 2d, denoted as M-phase). The fast Fourier transform (FFT) images of M-phase in Figure 2f and Figure S3b,c reveal the innermost six spots corresponding to the Moiré pattern with the lattice constant of ~30.40 Å, which is exactly 4 times the lattice constant of arsenic film. However, the other arsenic film with one edge along $[2\bar{3}\bar{1}]$ does not form a Moiré pattern (bottom part of Figure 2d, denoted as T-phase), demonstrating the same atomic structure as the M-phase (Figure 2e). To determine the atomic structure of this arsenic film, the high-resolution STM image of the arsenic films on Au(111) surface (Figure 2c) demonstrates a hexagonal lattice with a lattice constant of 7.60 Å. (The primitive unit cell is marked by the red diamond.) More specifically, the left half unit cell (HUC) has one bright and large protrusion, while the right HUC has three dim and small protrusions. Further, the arsenic film grown on HOPG surface (Figure S4) shows the same appearance in STM images. As shown in Figure 1f and Figure S4, we infer that this arsenic film is a molecular film of As_4 assembled by van der Waals forces rather than arsenene or arsenic alloy. This assignment is further supported by the following reasons: (i) The planar arsenic films can only be grown at low substrate temperatures (77−175 K). When it is grown on HOPG, it is less stable and can be easily affected by the STM tip during scanning (Figure S5). The above experimental results are against the high stability predicted by theoretical calculations for arsenene.[40,42] (ii) These arsenic films on Au(111) and HOPG possess the same atomic structure, indicating that the structure of the arsenic films is independent of the physical properties and crystallinity of the substrate. Additionally, the arsenic films show a large lattice constant of ~7.60 Å, approximately twice that of the arsenene, even though their apparent heights are rather close (Figure S6).[61,62] (iii) The evaporated source by direct heating of the gray arsenic chunk mainly consists of tetrahedral As_4 molecular vapor,[63] which cannot be cracked at low temperatures.

To further identify the structure of the As_4 molecular film, we performed the first-principles calculations to simulate the STM images. Arranging the tetrahedral As_4 molecules with one of their vertices alternatively pointing upward or downward on the surface as shown in Figure S7, the structure can be optimized on both Au(111) and HOPG surfaces. The simulated STM images (Figure S7) reveal that the upward

As_4 molecule appears as one big bright spot in the left HUC and the inverted As_4 molecule appears as three less bright spots in the right HUC, in agreement with the experimental images. The STS spectrum of the As_4 film on Au(111) surface is similar to that of Au(111) spectrum (Figure S8), due to the DOS contribution by Au substrate by the proximity effects.[64] In addition, the surface state of gold is shifted to −0.06 V, arising from the charge doping to the arsenic film from the gold substrate. Therefore, the As_4 molecular self-assembled monolayer film is governed by the intermolecular interactions (van der Waals forces),[65,66] as well as the molecule−substrate interactions induced by partial charge transfer,[67] which can be inferred from the various growth behaviors of arsenic on different substrates at low temperatures (Figure S11a,c,e,g).

Interestingly, arsenic nanochains can be grown on Au(111) when the temperature reaches above 175 K (Figure S9). Similar to the atomic chains produced by P and Sb,[21,29] high-density arsenic nanochains can be self-arranged into the ordered superstructure (Figure 1h and Figure S10). Surprisingly, these arsenic nanochains cannot be grown on HOPG, Ag(111), and Cu(111) surfaces even when the substrate temperature is varied over a wide range (Figure S11). It was observed that As_4 molecular films can be grown on HOPG at low temperatures (below 175 K), while no adsorption on this substrate occurs at high temperatures (Figure S11c,d). On Ag(111) substrate, arsenic prefers to form particles or clusters at low temperatures (below 300 K) and forms a hexagonal structure without nanochains at high temperatures of ~600 K (Figure S11e,f).[39] On Cu(111) substrate, only arsenic particles or clusters can be seen at various temperatures (Figure S11g,h). Therefore, we conclude that Au(111) surface is peculiar for the formation of periodic arsenic nanochains with large areas (Figure S11a,b), probably due to the surface-catalyzed decomposition of As_4 molecules on Au(111) together with its template effect.

To understand the role of Au(111) surface, we have adopted the climbing image nudged elastic band (CI-NEB) method[68] to search the energy barriers and the reaction pathways of As_4 decomposition. As shown in Figure 3a, despite the total energy of the system being reduced by ~0.978 eV when an adsorbed As_4 molecule is decomposed into a segment of an arsenic nanochain, the rate of As_4 decomposition on Au(111) surface is predominantly determined by an energy barrier (activation energy, ~282 meV) between the first two states. In stark contrast, the total energy of the system is lower by ~3.05 eV on HOPG surface for an adsorbed As_4 molecule than for a decomposed segment of arsenic chain, yielding a large energy barrier (~2.77 eV) for the decomposition to occur (Figure 3b). The decomposition rate is related to several parameters as shown in the following equation:[69]

$$k \propto T\, e^{-E_a/(k_B T)} \tag{1}$$

where E_a, k_B, and T are the activation energy, Boltzmann constant, and absolute temperature, respectively. Hence, the decomposition rate on Au(111) surface is much higher (~10^{71} times) than that on HOPG surface at 175 K, revealing that the As_4 molecules practically do not decompose on HOPG surface, in excellent agreement with our experimental observations (Figure S11). Moreover, the substrate temperature plays an important role in the decomposition of As_4 molecule. Even on Au(111) surface, the decomposition rate at 250 K is ~400 times that at 175 K, consistent with the observation of nanochains at relatively high temperatures. These calculations
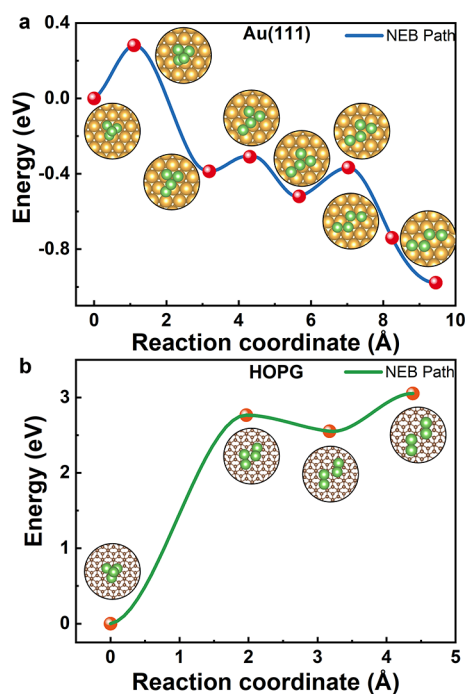
Figure 3. Surface-assisted effect of Au(111) on the decomposition of As$_4$ molecules. (a) Calculated minimum energy path of As$_4$ decomposition on Au(111) surface. (b) Energy path of As$_4$ decomposition on HOPG surface. The energy barriers of the first step of As$_4$ decomposition are ~0.282 and ~2.77 eV, respectively. The total energy of the system is reduced by ~0.978 eV on Au(111) surface but is raised by ~3.05 eV on HOPG surface after As$_4$ decomposition.

demonstrate that As$_4$ decomposition can proceed readily at elevated temperature to form 1D nanochain presumably due to the surface catalysis and template effect of Au(111) surface. Unlike Au(111) substrate, Ag(111) and Cu(111) substrates are not suitable for the growth of As chain. As shown in Figure S12, the total energy of the system is reduced only by ~0.278 eV, demonstrating that the interaction between Ag(111) and arsenic segment is very weak. On the contrary, the total energy of the system is significantly reduced by ~1.583 eV on Cu(111), implying that there is a strong Cu−As bonding interaction leading to the possible formation of Cu−As surface alloy. Therefore, the above results demonstrate that Au(111) substrate plays an important role in the decomposition of As$_4$ molecules to form 1D nanochains. Moreover, the growth mode of 1D As nanochains (Figure S1a) is also different from the etching effect in the growth of P on Au(111).[59,60]

When the substrate temperature is raised higher than 250 K, we can only observe arsenic nanochains without planar As$_4$ molecular films on Au(111) surface as illustrated in Figure 4a. The high-resolution STM image of arsenic nanochains in Figure 4b reveals an armchair-like structure with unit cell dimensions of 5.70 Å × 8.60 Å, indicating that arsenic nanochains tend to self-organize to form a (2 × 3) superstructure of Au(111) surface extending over a surface area of tens of thousands square nanometers, despite the presence of some structural imperfections arising from the reconstruction of Au(111) surface.[70] Compared to the long-length 1D P nanochains grown on Ag(111) surface with similar unit cell dimensions and chain shifts, the length of an individual As nanochain disrupted by the boundaries of

Au(111) surface construction is ~31.4 Å, nearly half of the unit cell size of Au(111) surface construction (63 Å).[21,71,72] DFT calculations were then performed to reveal the experimentally identified structure. The structural model displayed in Figure 4c shows the array of arsenic chains after full relaxation of the system. The simulated STM image from this structural model (Figure 4d) shows good agreement with the experimental image.

Figure 4e shows the calculated density of states (DOS) of a freestanding arsenic nanochain and gold-supported arsenic nanochain. In detail, the occupied states of the freestanding arsenic nanochains are dominantly contributed by the s, p$_x$, and p$_y$ orbitals of arsenic and the unoccupied states are mainly contributed by the p$_z$ orbital, resulting in a narrow bandgap of ~0.5 eV (Figure 4e,g and Figure S13). However, the DOS of the Au-supported arsenic nanochains shown in Figure 4e demonstrates that the electronic states around the Fermi level are contributed mainly by the arsenic out-of-plane p$_z$ orbital rather than the in-plane s, p$_x$, and p$_y$ orbitals. The overlaps of As p$_z$ orbital and Au d orbitals (Figure S14) lead to a metallic character for the Au-supported arsenic nanochains. In addition, the states contributed by the As p$_z$ and p$_x$ orbitals in the Au-supported arsenic nanochains are shifted to appeoximately −0.54 eV, implying that the electron transfer from Au substrate to arsenic nanochains leads to the n-doping for arsenic nanochains. The P1 (−1.07 eV) and P2 (1.06 eV) peaks in Figure 4e are mainly contributed by As p orbitals. The typical STS spectrum recorded on the Au-supported arsenic nanochains in Figure 4f presents a metallic character, consistent with the theoretical results. Meanwhile, since two prominent peaks at −1.0 and 1.13 V show the same energy difference (2.13 eV) as the theoretical results, we suppose that these two peaks are associated with the theoretically calculated P1 and P2 states, respectively. Figure 4k,i shows dI/dV maps recorded at the biases corresponding to the energy positions of P1 and P2 states, respectively. The middle region between two neighboring nanochains in both dI/dV maps exhibits high DOS possibly due to the contribution by underlying Au substrate, while the signals acquired at 1.13 and −1.0 V in the chain region reveal different periodic localized patterns, indicating the various orbital-associated electronic states. Furthermore, the I−V spectra taken on the Au-supported arsenic nanochains with various tip heights are displayed in Figure S15a.[73] The corresponding dI/dV spectra in Figure S15b demonstrate that the peaks of P1 and P2 can still be clearly seen while, due to the reduced wave function coupling between the tip and the As p$_z$ orbital/Au d orbitals, the DOS around the Fermi level decreases more quickly with the increase of tip height, revealing that both the DOS of Au and charge transfer have significant impacts on the electronic structures of Au-supported arsenic nanochains. Moreover, the differential conductance map (Figure 4l) recorded shows no distinct features, indicating the hybridization between As nanochains and Au(111) substrate by proximity effects.[64]

To evaluate the binding between the arsenic nanochains and Au(111) substrate, we have performed tip indentation and manipulation to attempt to flip the chains that can create a bilayer structure (Figure 5a). The period along the nanochain (~5.70 Å), matching two times the lattice constant along Au[110] direction (2.88 Å), is likely to be an important driving force for the formation of the ordered (2 × 3)-superstructure arsenic nanochains. However, as shown in Figure 5b,c, the arsenic nanochains could be peeled off by the tip indentation
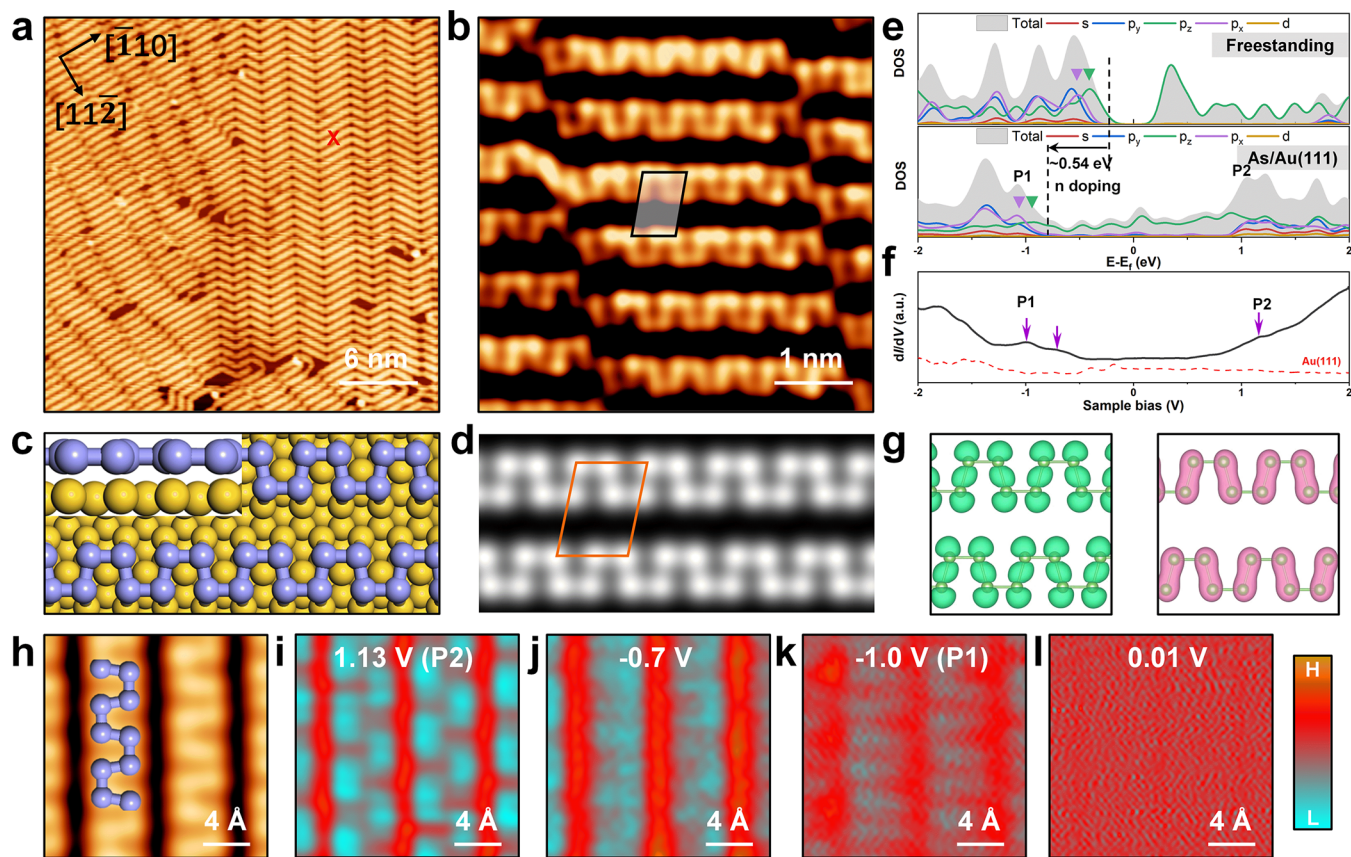
Figure 4. Structural and electronic properties of arsenic nanochains. (a) Large-scale STM image (V_{bias} = 100 mV, I_t = 1 nA) and (b) high-resolution STM image (V_{bias} = −5 mV, I_t = 5 nA) of parallel arsenic chains on Au(111), whose unit cell marked by the black rhombus is 5.70 Å × 8.60 Å. (c) Top view of structural model of arsenic nanochains on Au(111) surface. The inset is the side view image. (d) Simulated STM images of arsenic nanochains. (e) Calculated total and partial DOS for the freestanding and Au-supported arsenic nanochain. The DOS of the freestanding arsenic nanochain by directly removing the gold substrate in the relaxed As nanochain/Au(111). (f) Experimental dI/dV spectra of arsenic nanochains at the labeled position in (a) and Au(111) substrate. (g) Band decomposed charge density of valence band maximum (green) and conduction band minimum (red), respectively. (h−l) High-resolution STM image (V_{bias} = 10 mV, I_t = 1 nA) of arsenic chains and corresponding dI/dV maps recorded at different energy positions [1.13 V for (i), −0.7 V for (j), −1.0 V (k), and 10 mV for (l)].

into the Au(111) substrate with various depths. Several arsenic nanochains were flipped in the vicinity of the pits produced by tip indentation (Figure 5d,e and Figure S16). The atomic structure and lattice constant of the flipped arsenic nanochains were the same as the underneath surface (in the inset of Figure 5d,e), indicating the possibility of exfoliating or transferring the arsenic nanochains for the fabrication of the nanodevices. Furthermore, the STS recorded on the bilayer nanochains (Figure S17) also reveals the metallic properties, perhaps due to the interaction between the top and bottom arsenic nanochains, which is confirmed by the theoretical calculations (Figure S18).

Unlike the theoretically predicted structures of arsenic nanochains,[31,40,42] which usually possess buckled or puckered honeycomb lattice cut from gray or black arsenic monolayers, respectively, the in-plane armchair arsenic nanochains formed on Au(111) surface have not been reported before. In addition, the geometric properties of arsenic nanochains are different from the buckled arsenene grown on Ag(111) surface[39] but similar to the phosphorene chains formed on Ag(111) surface,[21] while the antimonene nanochains on Ag(111) surface cannot form ordered structure.[29] Unexpectedly, the bandgap of the arsenic nanochains is much smaller than the predicted bandgap of nonflat arsenene or arsenene NRs.[31,40,42] The narrower bandgap of the arsenic nanochains offers great

potential for the applications in nanoelectronics and infrared optoelectronics. However, the stability test of As nanochains (Figure S19) reveals that the As nanochains are stable when exposed to O_2 under UHV conditions but unstable when exposed to air perhaps due to their sensitivity to other atmospheric species, e.g., H_2O.[74] Therefore, the fabrication of the practical devices requires a clean environment with a low humidity.

CONCLUSION

In summary, we have demonstrated the temperature-dependent formation of arsenic nanostructures on Au(111) surface, including arsenic molecular films and nanochains. The arsenic film grown at low temperature (≤175 K) was a molecular layer formed by arranging the tetrahedral As_4 molecules with one of their vertices alternatively pointing upward or downward on the surface. The large areas of armchair-like arsenic nanochains were grown at substrate temperatures above 250 K. Due to the overlaps of As p_z orbital and Au d orbitals, the DOS of Au-supported arsenic nanochains exhibited a metallic character. By removing the influence of gold substrate, the freestanding armchair arsenic nanochain showed a semiconducting character with a small bandgap of ~0.50 eV, suitable for the applications of electronic and infrared optoelectronic devices. Furthermore, the flip of arsenic nanochains by tip indentation
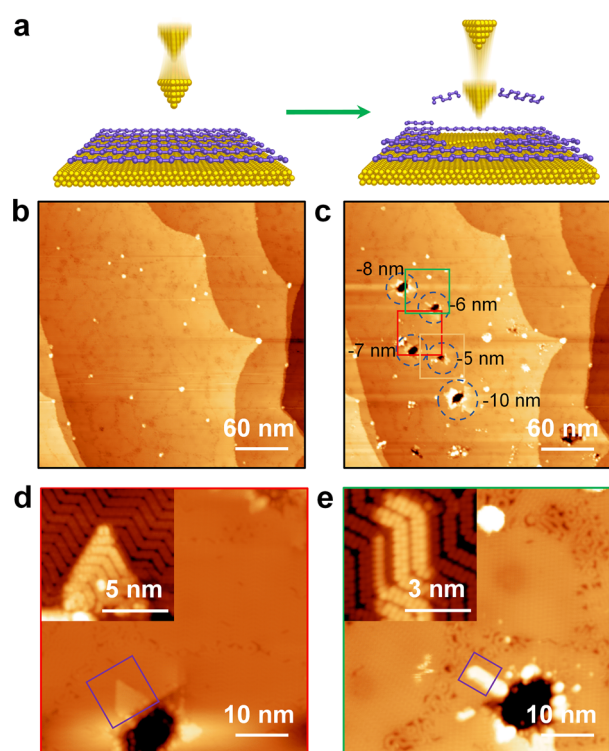
Figure 5. Flip the arsenic nanochains to form the bilayer structure via controlled tip indentation and manipulation. (a) Schematic illustration for tip indentation and manipulation of arsenic nanochains. To ensure the tip scanning without damage, the tip indentation depth is controlled to be larger than 5 nm. (b, c) Large-scale STM images (V_{bias} = 2 V, I_t = 100 pA) of arsenic nanochains before and after tip indentation into the Au(111) substrate with various depths. (d, e) Zoomed in images (V_{bias} = 2 V, I_t = 100 pA) of the squares in (c). Inset: high resolution images of the flipped arsenic nanochains [V_{bias} = 0.1 V, I_t = 5 nA in (d) and V_{bias} = 5 mV, I_t = 9 nA in (e)].

and manipulation demonstrates the feasible exfoliation or transfer of arsenic nanochains for future nanodevice fabrications. Our work not only can enrich the family of arsenic nanostructures for exploring low-dimensional physics and developing nanodevices but also can shed light on two directions for the growth of arsenene. One method is to find a suitable substrate which can assist the decomposition of As_4 molecules into arsenic atoms. Another method is to utilize an arsenic cracker source to directly produce arsenic dimers, even arsenic single atoms,[63] for the growth of arsenene on a wide range of substrates.

METHODS

Experiments. Our experiments were conducted with a commercial ultrahigh vacuum (UHV) low-temperature STM (Unisoku and Scienta Omicron Co., Ltd.) at a base pressure better than 1×10^{-10} mbar. A single crystalline Au(111) (MaTecK) was cleaned by Ar$^+$ sputtering and annealed at 800 K repeatedly. Arsenic granules (99.9999%, Prmat) were loaded in a Knudson cell. The Au(111) substrate was kept at various set temperatures during the deposition of arsenic. The evaporating temperature of arsenic was about 455 K, and the pressure during evaporation was 1×10^{-9} mbar approximately. After arsenic deposition, the sample was immediately transferred to the STM chamber for characterization. The tungsten tip was heated to 1300 K by electron beam (EB) heater and modified on a clean Au(111) surface prior to use. All the STM images were recorded in constant current mode at 4.8 K and processed with the

WSXM software.[75] STS spectra were obtained by directly recording differential conductance signals using the lock-in technique (the amplitude of 20 mV and the frequency at 431.231 Hz) at 4.8 K. dI/dV maps were measured using the same parameter as spectra in a constant-current mode.

Calculations. All the first-principles calculations were performed by the Vienna *ab initio* simulation package (VASP).[76,77] The electron−ion interactions were described by the projector-augmented wave (PAW) method,[78] and we chose the Perdew−Burke−Ernzerhof (PBE) functional within the generalized gradient approximation (GGA) to treat the exchange−correlation interaction of electrons.[79] The energy cutoff was set to 450 eV. The climbing image nudged elastic band (CI-NEB) method was used to search the energy barriers and reaction pathways.[68] In order to avoid the influence of the periodicity in the z direction, the vacuum layers of all models are set to 20 Å. The Brillouin zone was sampled with a γ-centered mesh with a $5 \times 5 \times 1$ k-point for geometry optimization and a denser $9 \times 9 \times 1$ k-mesh for electronic states calculations. The simulated STM images are produced using the Tersoff−Hamann scheme,[80] where the isovalue ρ_{iso} = 5×10^{-5} e/bohr^3 is used in all calculations.[81] The T-phase is a $\sqrt{7} \times \sqrt{7}$ $R19.1°$ supercell containing 2 As_4 molecules and 5 layers of gold, while the M-phase is an 11×11 supercell containing 32 As_4 molecules and 3 layers of gold. The structural model of arsenic nanochain on Au(111) surface is a 2×3 supercell containing 30 Au atoms and 4 As atoms. The As/HOPG is a 3×3 supercell containing 2 As_4 molecules and 2 layers of graphene. All atoms were fully relaxed to ensure the forces acting on each atom were below 0.01 eV/Å and the convergence criterion of the total energy was 10^{-6} eV. VASPKIT is helpful to analyze calculations from the VASP code.[82]

ASSOCIATED CONTENT

Ⓢ Supporting Information

The Supporting Information is available free of charge at https://pubs.acs.org/doi/10.1021/acsnano.2c07361.

STM image of arsenic segments on Au(111) surface; large-scale STM image of arsenic structure on Au(111) surface under high temperature; coexistence of M-phase and T-phase; As_4 molecular films on HOPG surface; continuous large-scale STM images of arsenic films on HOPG; line profiles of As films on Au(111) surface; calculations of As_4 molecular films on Au(111) and HOPG surfaces; STS spectrum of arsenic film on Au(111); large-scale STM image of arsenic deposited on Au(111) substrate from 175 to 250 K; comparison of group-VA nanochains; arsenic structures grown on various substrates at low and high temperatures; the total energy difference between an As_4 molecule and arsenic segment on Ag(111) and Cu(111) surfaces; calculated DOS of freestanding arsenic nanochain with relaxation; calculated DOS of the relaxed arsenic nanochains; STS on arsenic nanochains with various tip heights; zoomed in STM image; STS of bilayer arsenic nanochains; calculations of bilayer arsenic nanochains on Au(111) substrate; stability of As nanostructures (PDF)

AUTHOR INFORMATION

Corresponding Authors

Yaping Ma − *Key Laboratory of Quantum Matt Science, Henan Key Laboratory of Photovoltaic Materials, Henan University, Kaifeng, Henan 475004, China; School of Physical Science and Technology and Key Laboratory of Artificial Micro- and Nano-Structures of Ministry of Education, Wuhan University, Wuhan, Hubei 430072,*

China; ⓘ orcid.org/0000-0003-3907-6881;
Email: mustc@henu.edu.cn

Hu Xu − *Department of Physics, Southern University of Science and Technology, Shenzhen, Guangdong 518055, China;* ⓘ orcid.org/0000-0002-2254-5840; Email: xuh@sustech.edu.cn

Kedong Wang − *Department of Physics, Southern University of Science and Technology, Shenzhen, Guangdong 518055, China;* ⓘ orcid.org/0000-0003-1253-5603; Email: wangkd@sustech.edu.cn

Xudong Xiao − *School of Physical Science and Technology and Key Laboratory of Artificial Micro- and Nano-Structures of Ministry of Education, Wuhan University, Wuhan, Hubei 430072, China;* Email: xdxiao@whu.edu.cn

Authors

Guowei Liu − *Department of Physics, Southern University of Science and Technology, Shenzhen, Guangdong 518055, China; School of Physical Science and Technology and Key Laboratory of Artificial Micro- and Nano-Structures of Ministry of Education, Wuhan University, Wuhan, Hubei 430072, China;* ⓘ orcid.org/0000-0003-1283-788X

Shao-Gang Xu − *Department of Physics, Southern University of Science and Technology, Shenzhen, Guangdong 518055, China*

Xiji Shao − *Department of Physics, Southern University of Science and Technology, Shenzhen, Guangdong 518055, China*

Wenqi Xiong − *School of Physical Science and Technology and Key Laboratory of Artificial Micro- and Nano-Structures of Ministry of Education, Wuhan University, Wuhan, Hubei 430072, China*

Xuefeng Wu − *Department of Physics, Southern University of Science and Technology, Shenzhen, Guangdong 518055, China; School of Physical Sciences, Great Bay University, Dongguan 523000, China*

Shuxuan Zhang − *Department of Physics, Southern University of Science and Technology, Shenzhen, Guangdong 518055, China*

Chenwei Liao − *Department of Physics, Southern University of Science and Technology, Shenzhen, Guangdong 518055, China*

Congrun Chen − *Department of Physics, Southern University of Science and Technology, Shenzhen, Guangdong 518055, China*

Xixian Wang − *Department of Physics, Southern University of Science and Technology, Shenzhen, Guangdong 518055, China*

Shengjun Yuan − *School of Physical Science and Technology and Key Laboratory of Artificial Micro- and Nano-Structures of Ministry of Education, Wuhan University, Wuhan, Hubei 430072, China;* ⓘ orcid.org/0000-0001-6208-1502

Weifeng Zhang − *Key Laboratory of Quantum Matt Science, Henan Key Laboratory of Photovoltaic Materials, Henan University, Kaifeng, Henan 475004, China*

Jiong Lu − *Department of Chemistry and Institute for Functional Intelligent Materials, National University of Singapore, 117543, Singapore;* ⓘ orcid.org/0000-0002-3690-8235

Complete contact information is available at:
https://pubs.acs.org/10.1021/acsnano.2c07361

Author Contributions

Notes

The authors declare no competing financial interest.

ACKNOWLEDGMENTS

REFERENCES

(1) Liu, Y.; Huang, Y.; Duan, X. Van Der Waals Integration before and Beyond Two-Dimensional Materials. *Nature* **2019**, *567*, 323−333.

(2) Zhang, S.; Guo, S.; Chen, Z.; Wang, Y.; Gao, H.; Gomez-Herrero, J.; Ares, P.; Zamora, F.; Zhu, Z.; Zeng, H. Recent Progress in 2D Group-VA Semiconductors: From Theory to Experiment. *Chem. Soc. Rev.* **2018**, *47*, 982−1021.

(3) Pizzi, G.; Gibertini, M.; Dib, E.; Marzari, N.; Iannaccone, G.; Fiori, G. Performance of Arsenene and Antimonene Double-Gate Mosfets from First Principles. *Nat. Commun.* **2016**, *7*, 12585.

(4) Sun, Y.; Gao, S.; Xie, Y. Atomically-Thick Two-Dimensional Crystals: Electronic Structure Regulation and Energy Device Construction. *Chem. Soc. Rev.* **2014**, *43*, 530−546.

(5) Ma, Y.; Shao, X.; Li, J.; Dong, B.; Hu, Z.; Zhou, Q.; Xu, H.; Zhao, X.; Fang, H.; Li, X.; et al. Electrochemically Exfoliated Platinum Dichalcogenide Atomic Layers for High-Performance Air-Stable Infrared Photodetectors. *ACS Appl. Mater. Interfaces* **2021**, *13*, 8518−8527.

(6) Zhang, Y.; Tan, Y.-W.; Stormer, H. L.; Kim, P. Experimental Observation of the Quantum Hall Effect and Berry's Phase in Graphene. *Nature* **2005**, *438*, 201−204.

(7) Novoselov, K. S.; Geim, A. K.; Morozov, S. V.; Jiang, D.; Katsnelson, M. I.; Grigorieva, I.; Dubonos, S.; Firsov, a. Two-Dimensional Gas of Massless Dirac Fermions in Graphene. *Nature* **2005**, *438*, 197−200.

(8) Mannix, A. J.; Kiraly, B.; Hersam, M. C.; Guisinger, N. P. Synthesis and Chemistry of Elemental 2D Materials. *Nat. Rev. Chem.* **2017**, *1*, 0014.

(9) Molle, A.; Goldberger, J.; Houssa, M.; Xu, Y.; Zhang, S.-C.; Akinwande, D. Buckled Two-Dimensional Xene Sheets. *Nat. Mater.* **2017**, *16*, 163−169.

(10) Glavin, N. R.; Rao, R.; Varshney, V.; Bianco, E.; Apte, A.; Roy, A.; Ringe, E.; Ajayan, P. M. Emerging Applications of Elemental 2D Materials. *Adv. Mater.* **2020**, *32*, 1904302.

(11) Grazianetti, C.; Martella, C.; Molle, A. The Xenes Generations: A Taxonomy of Epitaxial Single-Element 2D Materials. *Phys. Status Solidi-R* **2020**, *14*, 1900439.

(12) Manzeli, S.; Ovchinnikov, D.; Pasquier, D.; Yazyev, O. V.; Kis, A. 2D Transition Metal Dichalcogenides. *Nat. Rev. Mater.* **2017**, *2*, 17033.

(13) Tao, L.; Cinquanta, E.; Chiappe, D.; Grazianetti, C.; Fanciulli, M.; Dubey, M.; Molle, A.; Akinwande, D. Silicene Field-Effect Transistors Operating at Room Temperature. *Nat. Nanotechnol.* **2015**, *10*, 227−231.

(14) Mannix, A. J.; Zhou, X.-F.; Kiraly, B.; Wood, J. D.; Alducin, D.; Myers, B. D.; Liu, X.; Fisher, B. L.; Santiago, U.; Guest, J. R.; et al. Synthesis of Borophenes: Anisotropic, Two-Dimensional Boron Polymorphs. *Science* **2015**, *350*, 1513−1516.

(15) Derivaz, M.; Dentel, D.; Stephan, R.; Hanf, M.-C.; Mehdaoui, A.; Sonnet, P.; Pirri, C. Continuous Germanene Layer on Al (111). *Nano Lett.* **2015**, *15*, 2510−2516.

(16) Liu, H.; Neal, A. T.; Zhu, Z.; Luo, Z.; Xu, X.; Tománek, D.; Ye, P. D. Phosphorene: An Unexplored 2D Semiconductor with a High Hole Mobility. *ACS Nano* **2014**, *8*, 4033−4041.

(17) Que, Y.; Liu, B.; Zhuang, Y.; Xu, C.; Wang, K.; Xiao, X. On-Surface Synthesis of Graphene Nanoribbons on Two-Dimensional Rare Earth−Gold Intermetallic Compounds. *J. Phys. Chem. Lett.* **2020**, *11*, 5044−5050.

(18) Ruffieux, P.; Wang, S.; Yang, B.; Sánchez-Sánchez, C.; Liu, J.; Dienel, T.; Talirz, L.; Shinde, P.; Pignedoli, C. A.; Passerone, D.; et al. On-Surface Synthesis of Graphene Nanoribbons with Zigzag Edge Topology. *Nature* **2016**, *531*, 489−492.

(19) Cai, J.; Pignedoli, C. A.; Talirz, L.; Ruffieux, P.; Söde, H.; Liang, L.; Meunier, V.; Berger, R.; Li, R.; Feng, X.; et al. Graphene Nanoribbon Heterojunctions. *Nat. Nanotechnol.* **2014**, *9*, 896−900.

(20) Cai, J.; Ruffieux, P.; Jaafar, R.; Bieri, M.; Braun, T.; Blankenburg, S.; Muoth, M.; Seitsonen, A. P.; Saleh, M.; Feng, X.; et al. Atomically Precise Bottom-up Fabrication of Graphene Nanoribbons. *Nature* **2010**, *466*, 470−473.

(21) Zhang, W.; Enriquez, H.; Tong, Y.; Mayne, A. J.; Bendounan, A.; Smogunov, A.; Dappe, Y. J.; Kara, A.; Dujardin, G.; Oughaddou, H. Flat Epitaxial Quasi-1D Phosphorene Chains. *Nat. Commun.* **2021**, *12*, 5160.

(22) Watts, M. C.; Picco, L.; Russell-Pavier, F. S.; Cullen, P. L.; Miller, T. S.; Bartuś, S. P.; Payton, O. D.; Skipper, N. T.; Tileli, V.; Howard, C. A. Production of Phosphorene Nanoribbons. *Nature* **2019**, *568*, 216−220.

(23) Liu, Z.; Sun, Y.; Cao, H.; Xie, D.; Li, W.; Wang, J.; Cheetham, A. K.; et al. Unzipping of Black Phosphorus to Form Zigzag-Phosphorene Nanobelts. *Nat. Commun.* **2020**, *11*, 3917.

(24) Yang, Y.-R.; Zhang, Z.-Q.; Gu, L.; Fu, H.-H. Spin-Dependent Seebeck Effect in Zigzag Black Phosphorene Nanoribbons. *RSC adv.* **2016**, *6*, 44019−44023.

(25) Wu, Q.; Shen, L.; Yang, M.; Cai, Y.; Huang, Z.; Feng, Y. P. Electronic and Transport Properties of Phosphorene Nanoribbons. *Phys. Rev. B* **2015**, *92*, 035436.

(26) Yang, G.; Xu, S.; Zhang, W.; Ma, T.; Wu, C. Room-Temperature Magnetism on the Zigzag Edges of Phosphorene Nanoribbons. *Phys. Rev. B* **2016**, *94*, 075106.

(27) Taghizadeh Sisakht, E.; Fazileh, F.; Zare, M.; Zarenia, M.; Peeters, F. Strain-Induced Topological Phase Transition in Phosphorene and in Phosphorene Nanoribbons. *Phys. Rev. B* **2016**, *94*, 085417.

(28) Rathore, J.; Mahapatra, S. Formation of Antimonene Nanoribbons by Molecular Beam Epitaxy. *2D Mater.* **2020**, *7*, 045003.

(29) Mao, Y. H.; Zhang, L. F.; Wang, H. L.; Shan, H.; Zhai, X. F.; Hu, Z. P.; Zhao, A. D.; Wang, B. Epitaxial Growth of Highly Strained Antimonene on Ag(111). *Front. Phys.* **2018**, *13*, 138106.

(30) Tsai, H.-S.; Chen, C.-W.; Hsiao, C.-H.; Ouyang, H.; Liang, J.-H. The Advent of Multilayer Antimonene Nanoribbons with Room Temperature Orange Light Emission. *Chem. Commun.* **2016**, *52*, 8409−8412.

(31) Wang, Y.; Ding, Y. Electronic Structure and Carrier Mobilies of Arsenene and Antimonene Nanoribbons: A First-Principle Study. *Nanoscale Res. Lett.* **2015**, *10*, 254.

(32) Ares, P.; Palacios, J. J.; Abellán, G.; Gómez-Herrero, J.; Zamora, F. Recent Progress on Antimonene: A New Bidimensional Material. *Adv. Mater.* **2018**, *30*, 1703771.

(33) Touski, S. B.; López-Sancho, M. P. Effects of Vertical Electric Field and Charged Impurities on the Spin-Polarized Transport of B-Antimonene Armchair Nanoribbons. *Phys. Rev. B* **2021**, *103*, 115433.

(34) van Veen, E.; Yu, J.; Katsnelson, M. I.; Roldán, R.; Yuan, S. Electronic Structure of Monolayer Antimonene Nanoribbons under out-of-Plane and Transverse Bias. *Phys. Rev. Mater.* **2018**, *2*, 114011.

(35) Song, Y.; Wang, X.; Mi, W. Spin Splitting and Electric Field Modulated Electron-Hole Pockets in Antimonene Nanoribbons. *npj Quantum Mater.* **2017**, *2*, 15.

(36) Srivastava, P.; Abhishek; Sharma, V.; Jaiswal, N. K. First-Principles Investigation of Antimonene Nanoribbons for Sensing Toxic NO$_2$ Gas. *Phys. Status Solidi B* **2020**, *257*, 2000034.

(37) Kong, X.; Li, L.; Leenaerts, O.; Liu, X.-J.; Peeters, F. M. New Group-V Elemental Bilayers: A Tunable Structure Model with Four-, Six-, and Eight-Atom Rings. *Phys. Rev. B* **2017**, *96*, 035123.

(38) Vishnoi, P.; Mazumder, M.; Pati, S. K.; Rao, C. N. R. Arsenene Nanosheets and Nanodots. *New J. Chem.* **2018**, *42*, 14091−14095.

(39) Shah, J.; Wang, W.; Sohail, H. M.; Uhrberg, R. I. G. Experimental Evidence of Monolayer Arsenene: An Exotic 2D Semiconducting Material. *2D Mater.* **2020**, *7*, 025013.

(40) Zhang, S.; Xie, M.; Li, F.; Yan, Z.; Li, Y.; Kan, E.; Liu, W.; Chen, Z.; Zeng, H. Semiconducting Group 15 Monolayers: A Broad Range of Band Gaps and High Carrier Mobilities. *Angew. Chem., Int. Ed.* **2016**, *55*, 1666−9.

(41) Kamal, C.; Ezawa, M. Arsenene: Two-Dimensional Buckled and Puckered Honeycomb Arsenic Systems. *Phys. Rev. B* **2015**, *91*, 085423.

(42) Zhang, S.; Yan, Z.; Li, Y.; Chen, Z.; Zeng, H. Atomically Thin Arsenene and Antimonene: Semimetal−Semiconductor and Indi-rect−Direct Band-Gap Transitions. *Angew. Chem.* **2015**, *127*, 3155−3158.

(43) Zhang, P.; Ma, J.-Z.; Ishida, Y.; Zhao, L.-X.; Xu, Q.-N.; Lv, B.-Q.; Yaji, K.; Chen, G.-F.; Weng, H.-M.; Dai, X.; et al. Topologically Entangled Rashba-Split Shockley States on the Surface of Grey Arsenic. *Phys. Rev. Lett.* **2017**, *118*, 046802.

(44) Wang, Y.-P.; Ji, W.-X.; Zhang, C.-W.; Li, P.; Zhang, S.-F.; Wang, P.-J.; Li, S.-S.; Yan, S.-S. Two-Dimensional Arsenene Oxide: A Realistic Large-Gap Quantum Spin Hall Insulator. *Appl. Phys. Lett.* **2017**, *110*, 213101.

(45) Zhang, H.; Ma, Y.; Chen, Z. Quantum Spin Hall Insulators in Strain-Modified Arsenene. *Nanoscale* **2015**, *7*, 19152−19159.

(46) Kong, X.; Gao, M.; Yan, X. W.; Lu, Z. Y.; Xiang, T. Superconductivity in Electron-Doped Arsenene. *Chin. Phys. B* **2018**, *27*, 046301.

(47) Gusmão, R.; Sofer, Z.; Bouša, D.; Pumera, M. Pnictogen (as, Sb, Bi) Nanosheets for Electrochemical Applications Are Produced by Shear Exfoliation Using Kitchen Blenders. *Angew. Chem.* **2017**, *129*, 14609−14614.

(48) Sheng, F.; Hua, C.; Cheng, M.; Hu, J.; Sun, X.; Tao, Q.; Lu, H.; Lu, Y.; Zhong, M.; Watanabe, K.; et al. Rashba Valleys and Quantum Hall States in Few-Layer Black Arsenic. *Nature* **2021**, *593*, 56−60.

(49) Seidl, M.; Balazs, G.; Scheer, M. The Chemistry of Yellow Arsenic. *Chem. Rev.* **2019**, *119*, 8406−8434.

(50) Mardanya, S.; Thakur, V. K.; Bhowmick, S.; Agarwal, A. Four Allotropes of Semiconducting Layered Arsenic That Switch into a Topological Insulator Via an Electric Field: Computational Study. *Phys. Rev. B* **2016**, *94*, 035423.

(51) García-Fuente, A.; Carrete, J.; Vega, A.; Gallego, L. J. Tunable Gap in Stable Arsenene Nanoribbons Opens the Door to Electronic Applications. *RSC adv.* **2019**, *9*, 11818−11823.

(52) Ao, L.; Pham, A.; Xiang, X.; Klose, F.; Li, S.; Zu, X. Tunable Electronic and Magnetic Properties of Arsenene Nanoribbons. *RSC Adv.* **2017**, *7*, 51935−51943.

(53) Tsai, H.-S.; Wang, S.-W.; Hsiao, C.-H.; Chen, C.-W.; Ouyang, H.; Chueh, Y.-L.; Kuo, H.-C.; Liang, J.-H. Direct Synthesis and Practical Bandgap Estimation of Multilayer Arsenene Nanoribbons. *Chem. Mater.* **2016**, *28*, 425−429.

(54) Chen, Y.; Chen, C.; Kealhofer, R.; Liu, H.; Yuan, Z.; Jiang, L.; Suh, J.; Park, J.; Ko, C.; Choe, H. S.; et al. Black Arsenic: A Layered

Semiconductor with Extreme in-Plane Anisotropy. *Adv. Mater.* **2018**, *30*, 1800754.

(55) Bhuvaneswari, R.; Nagarajan, V.; Chandiramouli, R. Recent Advances in Arsenene Nanostructures Towards Prediction, Properties, Synthesis and Applications. *Surf. Interfaces* **2022**, *28*, 101610.

(56) Hu, Y.; Liang, J.; Xia, Y.; Zhao, C.; Jiang, M.; Ma, J.; Tie, Z.; Jin, Z. 2D Arsenene and Arsenic Materials: Fundamental Properties, Preparation, and Applications. *Small* **2022**, *18*, 2104556.

(57) Wang, Y.; Kong, L.; Chen, C.; Cheng, P.; Feng, B.; Wu, K.; Chen, L. Realization of Regular-Mixed Quasi-1d Borophene Chains with Long-Range Order. *Adv. Mater.* **2020**, *32*, 2005128.

(58) Chen, C.; Lv, H.; Zhang, P.; Zhuo, Z.; Wang, Y.; Ma, C.; Li, W.; Wang, X.; Feng, B.; Cheng, P.; et al. Synthesis of Bilayer Borophene. *Nat. Chem.* **2022**, *14*, 25−31.

(59) Tian, H.; Zhang, J. Q.; Ho, W. K.; Xu, J. P.; Xia, B. W.; Xia, Y. P.; Fan, J.; Xu, H.; Xie, M. H.; Tong, S. Y. Two-Dimensional Metal-Phosphorus Network. *Matter* **2020**, *2*, 111−118.

(60) Golias, E.; Krivenkov, M.; Varykhalov, A.; Sanchez-Barriga, J.; Rader, O. Band Renormalization of Blue Phosphorus on Au(111). *Nano Lett.* **2018**, *18*, 6672−6678.

(61) Bhuvaneswari, R.; Nagarajan, V.; Chandiramouli, R. Recent Advances in Arsenene Nanostructures Towards Prediction, Properties, Synthesis and Applications. *Surf. Interfaces* **2022**, *28*, 101610.

(62) Luo, Z.; Han, D. D.; Dong, J. C.; Li, H. J.; Yu, W.; Zhang, S. D.; Zhang, X.; Wang, Y. Tunable Arsenene Band Gap in Arsenene/Graphene Heterostructures. *Jpn. J. Appl. Phys.* **2019**, *58*, SBBH01.

(63) Hao, Z.-B.; Ren, Z.-Y.; Guo, W.-P.; Luo, Y. Studies on Incorporation of As$_2$ and As$_4$ in III−V Compound Semiconductors with Two Group V Elements Grown by Molecular Beam Epitaxy. *J. Cryst. Growth* **2001**, *224*, 224−229.

(64) Lin, C.-L.; Arafune, R.; Kawahara, K.; Kanno, M.; Tsukahara, N.; Minamitani, E.; Kim, Y.; Kawai, M.; Takagi, N. Substrate-Induced Symmetry Breaking in Silicene. *Phys. Rev. Lett.* **2013**, *110*, 076801.

(65) Barth, J. V. Molecular Architectonic on Metal Surfaces. *Annu. Rev. Phys. Chem.* **2007**, *58*, 375−407.

(66) Kühnle, A. Self-Assembly of Organic Molecules at Metal Surfaces. *Curr. Opin. Colloid Interface Sci.* **2009**, *14*, 157−168.

(67) Lexow, M.; Maier, F.; Steinrück, H.-P.; et al. Ultrathin Ionic Liquid Films on Metal Surfaces: Adsorption, Growth, Stability and Exchange Phenomena. *Adv. Phys.: X* **2020**, *5*, 1761266.

(68) Henkelman, G.; Uberuaga, B. P.; Jónsson, H. A Climbing Image Nudged Elastic Band Method for Finding Saddle Points and Minimum Energy Paths. *J. Chem. Phys.* **2000**, *113*, 9901−9904.

(69) Nørskov, J. K.; Studt, F.; Abild-Pedersen; et al.Kinetics. *Fundamental Concepts in Heterogeneous Catalysis*; John Wiley & Sons: Hoboken, NJ, 2014; pp 68−84.

(70) Narasimhan, S.; Vanderbilt, D. Elastic Stress Domains and the Herringbone Reconstruction on Au (111). *Phys. Rev. Lett.* **1992**, *69*, 1564.

(71) Wöll, C.; Chiang, S.; Wilson, R.; Lippel, P. Determination of Atom Positions at Stacking-Fault Dislocations on Au (111) by Scanning Tunneling Microscopy. *Phys. Rev. B* **1989**, *39*, 7988.

(72) Barth, J. V.; Brune, H.; Ertl, G.; Behm, R. Scanning Tunneling Microscopy Observations on the Reconstructed Au (111) Surface: Atomic Structure, Long-Range Superstructure, Rotational Domains, and Surface Defects. *Phys. Rev. B* **1990**, *42*, 9307.

(73) Hu, S.; Zhao, A.; Kan, E.; Cui, X.; Zhang, X.; Ming, F.; Fu, Q.; Xiang, H.; Yang, J.; Xiao, X. Electrical Rectification by Selective Wave-Function Coupling in Small Ag Clusters on Si (111)−(7 × 7). *Phys. Rev. B* **2010**, *81*, 115458.

(74) Grazianetti, C.; Faraone, G.; Martella, C.; Bonera, E.; Molle, A. Embedding Epitaxial (Blue) Phosphorene in between Device-Compatible Functional Layers. *Nanoscale* **2019**, *11*, 18232−18237.

(75) Horcas, I.; Fernandez, R.; Gomez-Rodriguez, J. M.; Colchero, J.; Gomez-Herrero, J.; Baro, A. M. Wsxm: A Software for Scanning Probe Microscopy and a Tool for Nanotechnology. *Rev. Sci. Instrum.* **2007**, *78*, 013705.

(76) Kresse, G.; Furthmuller, J. Efficient Iterative Schemes for Ab Initio Total-Energy Calculations Using a Plane-Wave Basis Set. *Phys. Rev. B Condens. Matter* **1996**, *54*, 11169−11186.

(77) Kresse, G.; Furthmuller, J. Efficiency of Ab-Initio Total Energy Calculations for Metals and Semiconductors Using a Plane-Wave Basis Set. *Comput. Mater. Sci.* **1996**, *6*, 15−50.

(78) Blochl, P. E. Projector Augmented-Wave Method. *Phys. Rev. B Condens. Matter* **1994**, *50*, 17953−17979.

(79) Perdew, J. P.; Burke, K.; Ernzerhof, M. Generalized Gradient Approximation Made Simple (Vol 77, Pg 3865, 1996). *Phys. Rev. Lett.* **1997**, *78*, 1396−1396.

(80) Tersoff, J.; Hamann, D. R. Theory of the Scanning Tunneling Microscope. *Phys. Rev. B Condens. Matter* **1985**, *31*, 805−813.

(81) Gustafsson, A.; Okabayashi, N.; Peronio, A.; Giessibl, F. J.; Paulsson, M. Analysis of Stm Images with Pure and Co-Functionalized Tips: A First-Principles and Experimental Study. *Phys. Rev. B* **2017**, *96*, 085415.

(82) Wang, V.; Xu, N.; Liu, J.; et al. VASPKIT: A User-Friendly Interface Facilitating High-Throughput Computing and Analysis Using VASP Code. *Comput. Phys. Commun.* **2021**, *267*, 108033.

⧉ Recommended by ACS